

STRUCTURE NOTE

Crystal structure of lipoate-bound lipoate ligase 1, LipL1, from *Plasmodium falciparum*

Alfredo J. Guerra, Gustavo A. Afanador, and Sean T. Prigge *

¹Department of Molecular Microbiology and Immunology, Johns Hopkins Bloomberg School of Public Health, Baltimore, Maryland

ABSTRACT

Plasmodium falciparum lipoate protein ligase 1 (PfLipL1) is an ATP-dependent ligase that belongs to the biotin/lipoate A/B protein ligase family (PFAM PF03099). PfLipL1 is the only known canonical lipoate ligase in *Pf* and functions as a redox switch between two lipoylation routes in the parasite mitochondrion. Here, we report the crystal structure of a deletion construct of PfLipL1 (PfLipL1_{Δ243-279}) bound to lipoate, and validate the lipoylation activity of this construct in both an *in vitro* lipoylation assay and a cell-based lipoylation assay. This characterization represents the first step in understanding the redox dependence of the lipoylation mechanism in malaria parasites.

Proteins 2017; 85:1777–1783.
© 2017 Wiley Periodicals, Inc.

Key words: lipoate; malaria; lipoylation; lipoate ligase; *Plasmodium falciparum*; LipL1.

INTRODUCTION

In humans, malaria is caused by five species of Apicomplexan parasites, of which *Plasmodium falciparum* is the deadliest.^{1–3} The parasite's lifecycle includes a sexual reproductive stage in the mosquito vector and two asexual reproductive cycles in the human host, namely, the liver stage (asymptomatic) and the blood stage (symptomatic). The majority of available drugs target the blood stage,⁴ although recent findings suggest an increase of drug resistance in certain populations of parasites.^{3,5–7}

The rise in drug resistance has created a necessity for new viable drug targets for malaria treatment. Lipoate metabolism is one such pathway. Lipoate is an organosulfur cofactor for a small number of enzymes that are essential for malaria parasite survival.^{8,9} *P. falciparum* has two distinct organelles that contain independent pathways for lipoate metabolism.^{8,10} The apicoplast, a nonphotosynthetic plastid organelle, contains a biosynthetic pathway that is dispensable in the blood stage but

is essential for progression from the liver to the blood stage.^{10–12} In contrast to the apicoplast, the mitochondrion relies exclusively on lipoate scavenged from the host red blood cell and this pathway is essential for both the liver and blood stages.^{8,12,13} Treatment with lipoate

Additional Supporting Information may be found in the online version of this article.

A. J. Guerra's current address is Department of Microbiology and Immunology, University of Michigan, Ann Arbor, Michigan, USA

G. A. Afanador's current address is Department of Biochemistry, University of Texas Southwestern Medical Center, Dallas, Texas, USA

Grant sponsor: U.S. Department of Energy, Office of Science, Office of Basic Energy Sciences; grant number: DE-AC02-76SF00515; Grant sponsor: DOE Office of Biological and Environmental Research; Grant sponsor: National Institutes of Health, National Institute of General Medical Sciences; grant numbers: P41GM103393; R56 AI065853; R01 AI125534; F32 AI110028; Grant sponsor: Johns Hopkins Malaria Research Institute; Grant sponsor: Bloomberg Family Foundation.

*Correspondence to: Sean T. Prigge; Department of Molecular Microbiology and Immunology, Johns Hopkins Bloomberg School of Public Health, Baltimore, MD. E-mail: sprigge2@jhu.edu

Received 19 December 2016; Revised 4 May 2017; Accepted 17 May 2017
Published online 24 May 2017 in Wiley Online Library (wileyonlinelibrary.com). DOI: 10.1002/prot.25324

analog, 8-bromooctanoate or 6,8-dichlorooctanoate, results in parasite growth inhibition likely due to reduced substrate lipoylation.^{8,14}

There are three lipoylated enzymes in the parasite mitochondrion: the E2 component of the branched chain α -ketoacid dehydrogenase complex (BCDH, PF3D7_0303700), the E2 component of the α -ketoglutarate dehydrogenase complex (KDH, PF3D7_1320800), and the H-protein of the glycine cleavage system (PF3D7_1132900).^{9,14,15} The lipoylation of these three proteins occurs via a complex mechanism that involves two enzymes, *PfLipL1* (PF3D7_1314600) and *PfLipL2* (PF3D7_0923600). *PfLipL1* has been shown to be the only canonical lipoate ligase and is solely responsible for lipoylation of the H-protein—a reaction that only occurs when lipoate is in the oxidized ring form.¹⁴ The lipoylation of BDCDH and KDH requires both *PfLipL1* and *PfLipL2* as well as fully reduced lipoate (dihydrolipoate).¹⁴ Although the mechanistic implications of redox dependence in the parasite remain unclear, *PfLipL1* is the switch that senses the oxidation state of lipoate and determines which downstream enzymes will be lipoylated.¹⁶ As a first step in understanding the molecular determinants of lipoylation activity and redox sensing in *PfLipL1*, we determined the structure of lipoate-bound *PfLipL1* _{Δ 243–279}.

MATERIALS AND METHODS

Plasmid construction

Plasmid pMALcHT-*PfLipL1*¹⁴ was mutated to generate pMALcHT-*PfLipL1* _{Δ 259–269}, pMALcHT-*PfLipL1* _{Δ 254–274}, and pMALcHT-*PfLipL1* _{Δ 249–279} using the primers listed in Supporting Information, Table S1. Mutating the pMALcHT-*PfLipL1* _{Δ 249–279} plasmid using the primers listed in Supporting Information, Table S1 then generated the plasmid pMALcHT-*PfLipL1* _{Δ 243–279}. The pMALcHT plasmid encodes a maltose-binding protein (MBP) followed by a linker region composed of a tobacco etch virus (TEV) protease cut site and a six histidine affinity tag.¹⁷

Protein expression and purification

All constructs were transformed into BL21-Star (DE3) cells (Invitrogen) containing the pRIL plasmid isolated from BL21-CodonPlus-RIL cells (Agilent) and plasmid pRK586 encoding the Tobacco Etch Virus (TEV) protease as described.¹⁷ These cells produce a protein product fused to an amino-terminal hexahistidine tag. Two liters of TB media containing ampicillin, kanamycin, and chloramphenicol were inoculated with an overnight culture for an initial OD₆₀₀ of approximately 0.1. The cells were grown to mid log phase at 37°C and then the temperature was reduced to 20°C. Protein expression was induced with 0.4 mM isopropyl β -D-1-thiogalactopyranoside (IPTG) and the cells were harvested after 10 h.

Purification was performed as described previously for full-length *PfLipL1*.¹⁴ Briefly, *PfLipL1* variants were purified by immobilized metal ion chromatography followed by cation exchange chromatography and gel filtration chromatography. The first two steps of purification were performed on the same day to avoid proteolytic cleavage. Purified *PfLipL1* mutants were concentrated to approximately 5 mg·mL⁻¹ and stored at -80°C.

Protein crystallization and data collection

Lipoyl-*PfLipL1* _{Δ 243–279} complex was prepared by adding 1.2 mol equiv of lipoate and excess ATP to 5 mg·mL⁻¹ apo-*LipL1* _{Δ 243–279}. Original crystals were obtained from a screen set up with 200 nL of protein and 200 nL reservoir containing 100 mM HEPES, pH 7.0 and 1.5 M (NH₄)₂SO₄ using a Mosquito crystallization robot (TTP Labtech) and equilibrated at 20°C in a 96-well sitting drop Intelli-Plate[®] (Art Robbins Instruments). The crystallization condition was further optimized to obtain larger crystals with 1 μ L protein and 1 μ L reservoir containing 100 mM HEPES, pH 7.0, 1.5 M (NH₄)₂SO₄, and 20% ethylene glycol and equilibrated at 20°C on a 24–4 sitting drop Intelli-Plate[®] (Art Robbins Instruments). Crystals were mounted on a 0.2 mm cryoloop (Hampton Research) and flash frozen in liquid nitrogen for data collection. Data sets were collected at SSRL beam line 7–1 at 100 K and λ 1.127085 Å.

Structure determination

The crystals belonged to the P3₂21 space group with cell dimensions of $a = b = 120.24$ Å, $c = 134.92$ Å, $\alpha = \beta = 90^\circ$, and $\gamma = 120^\circ$. Data reduction and scaling were performed with XDS/XSCALE.^{18–20} The molecular replacement solution was obtained using alanine-substituted *Escherichia coli* LplA (*EcLplA*; PDB: 3A7A, chain A) N-terminal domain and C-terminal domain search models with the Phaser-MR module in PHENIX.^{21,22} Model building was performed in Coot²³ and refinement in PHENIX. Lipoate-bound *PfLipL1* _{Δ 243–279} was refined to a crystallographic R_{work} of 27.3% and an R_{free} of 30.2%. The final structure was analyzed with validation tools in MOLPROBITY.^{24,25} Protein sequence similarity and Z-scores were calculated using the Dali server.²⁶ Sequence alignments were performed using the Clustal algorithm in Jalview.^{27–29} Structural visualization was performed via PyMol.³⁰

In vitro lipoylation assay

Lipoylation assays were performed as previously described.¹⁴ Briefly, purified *PfLipL1* variants (1 μ M) were incubated in reaction buffer (100 mM Na/K phosphate at pH 7.5 and 150 mM NaCl) containing 2 mM ATP, 2 mM MgCl₂, 200 μ M *R*-lipoic acid, and 10 μ M H-protein. After a 1 h incubation at 37°C, reactions were

quenched with the addition of gel loading buffer and analyzed by Western blot. The SDS-PAGE gel was transferred to a nitrocellulose membrane, blocked with 5% milk in PBS for 30 min, and probed with 1:5000 rabbit polyclonal α -LA (Calbiochem) for 2 h in 1% milk/PBS at room temperature. The membrane was washed with PBS three times and then probed with 1:5000 donkey α -Rabbit IgG horseradish peroxidase (HRP) secondary antibody (GE Healthcare) in 1% milk/PBS overnight at 4°C. The membranes were visualized with ECL western substrate (Pierce) and exposed to film.

Cell-based lipoylation assay

Cell-based lipoylation was performed as previously described.¹⁴ Briefly, lipoylation-deficient *E. coli* strain JEG3 containing the pRIL plasmid was transformed with a plasmid containing the candidate lipoate ligase (pMALcHT-*PfLipL1*, pMALcHT-*PfLipL1* _{Δ 259–269}, pMALcHT-*PfLipL1* _{Δ 254–274}, pMALcHT-*PfLipL1* _{Δ 249–279}, or pMALcHT-*PfLipL1* _{Δ 243–279}). Cells were subsequently grown in LB medium with 1% glucose, 5 mM sodium succinate, 5 mM sodium acetate, 35 $\mu\text{g} \cdot \text{mL}^{-1}$ chloramphenicol, 100 $\mu\text{g} \cdot \text{mL}^{-1}$ ampicillin, and 200 μM *R*-lipoic acid. Twenty-milliliter cultures were grown to mid-log phase at 37°C and induced with 0.4 mM IPTG for 10 h at 20°C. Cells were harvested by centrifugation and resuspended with 0.5 mL of buffer containing 20 mM HEPES, 100 mM NaCl at pH 7.5 and lysed by sonication. Cell lysates were clarified by centrifugation at 16,000g and the supernatants were collected and resolved by SDS-PAGE (Invitrogen). Lipoylated proteins were visualized by Western blot as described above.

Accession code

The atomic coordinates and structure factors have been deposited in the Protein Data Bank as entry 5T8U.

RESULTS AND DISCUSSION

Overall structure

To further our understanding into the lipoylation mechanism in malaria parasite mitochondria, we crystallized *PfLipL1* _{Δ 243–279} in the presence of lipoate and excess ATP. The resulting crystals only contained lipoate bound in the active site presumably due to degradation of the lipoyl-AMP conjugate during the process of crystallization or trapping of the lipoyl-bound form in the crystal lattice. Lipoate-bound *PfLipL1* _{Δ 243–279} crystallized in the trigonal P3₂21 space group and has cell dimensions of $a = b = 120.24 \text{ \AA}$, $c = 134.92 \text{ \AA}$, $\alpha = \beta = 90^\circ$, and $\gamma = 120^\circ$ with two monomers per asymmetric unit. The structure was solved using an alanine-substituted model of *EcLplA* (PDB code 3A7A, chain A). The N-terminal domain (residues 1–243) and C-terminal domain (residues 250–337) were used as independent search models. Lipoyl-*PfLipL1* _{Δ 243–279} was refined to 2.3 Å resolution with an

Table I

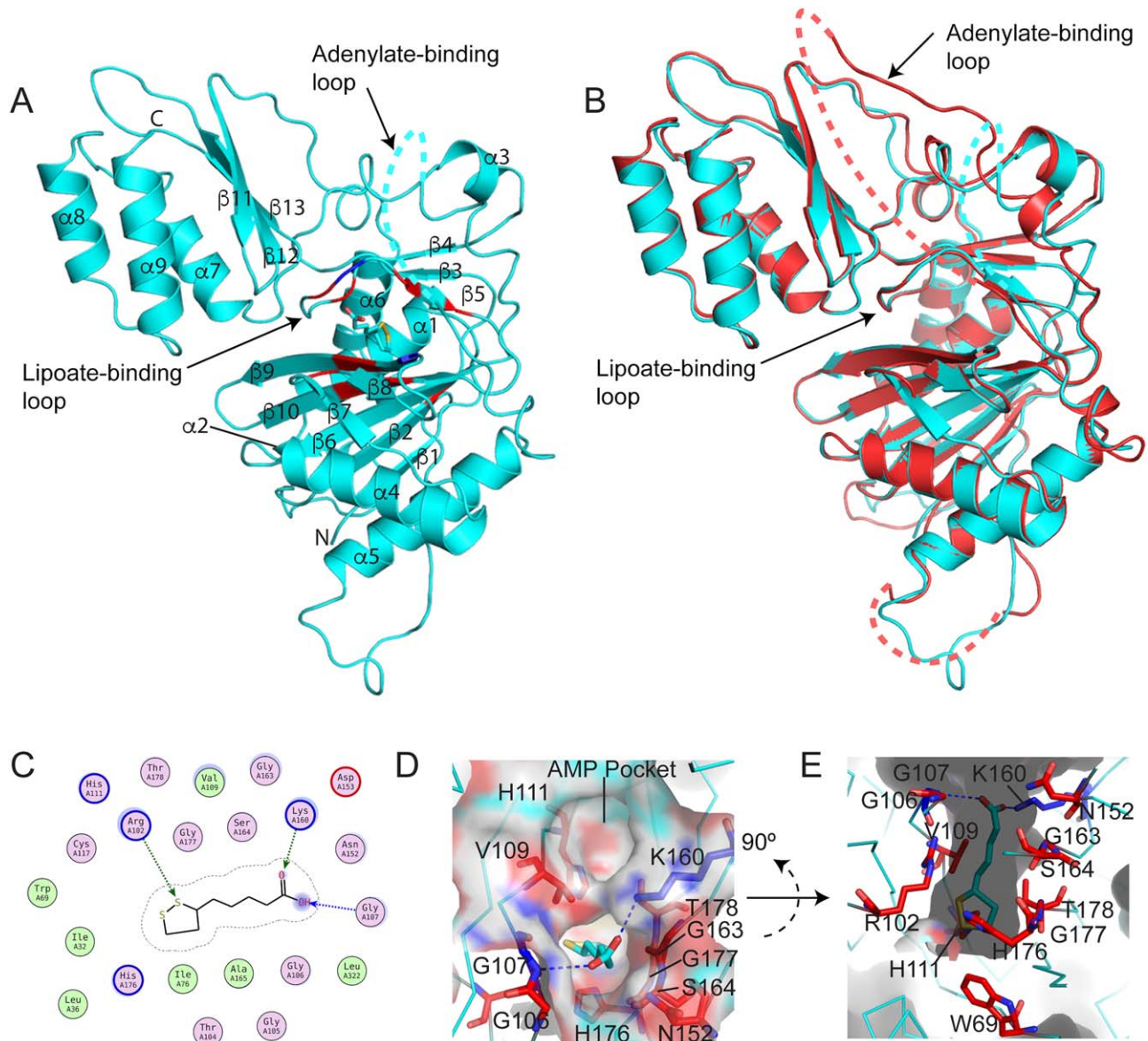
Data Collection and Refinement Statistics for Lipoate-Bound *PfLipL1* _{Δ 243–279}

Data Collection	
Resolution range (Å)	44.97–2.32 (2.41–2.32)
Total reflections	289251 (28279)
Unique reflections	48819 (4399)
Multiplicity	5.9 (5.8)
Completeness (%)	96.5 (90.4)
Mean I/sigma(I)	9.9 (0.6)
R-merge	0.139 (2.672)
CC1/2	0.998 (0.491)
CC*	0.999 (0.812)
Wilson B-factor (Å ²)	53.07
Space group	P 3 ₂ 2 1
Unit cell	
<i>a</i> , <i>b</i> , <i>c</i> (Å)	120.2, 120.2, 134.9
α , β , γ (°)	90, 90, 120
Refinement	
Reflections used in refinement	47298
Reflections used for R-free	2309
R-work (%)	27.28
R-free (%)	30.16
Molecules in asymmetric unit	2
Number of nonhydrogen atoms	5594
Macromolecules	5486
Ligands	24
Solvent	84
Protein residues	671
Ramachandran favored/outliers total (%)	624/1 95/0.15
Rotamer outliers (%)	0.33
Average B-factor (Å ²)	79.65
Macromolecules (Å ²)	80.06
Ligands (Å ²)	88.07
Solvent (Å ²)	50.41
RMS bonds (Å)/angles (°)	0.002/0.47
RMSZ bonds/angles	0.24/0.42

Statistics for the highest resolution shell are shown in parentheses.

R_{work} of 27.28% and an R_{free} of 30.16%. The crystallographic data and refinement statistics are summarized in Table I. The R_{free} value is high given the resolution but after multiple rounds of refinement taking into account various factors, such as restraints and B-factors, it was not possible to obtain a lower R_{free} value. Analysis of the data with PHENIX Xtriage and POINTLESS do not suggest contributions from twinning or translational non-crystallographic symmetry. Furthermore, analysis with ZANUDA in CCP4 is consistent with the P3₂21 space group used in this study.³¹ Thus, we hypothesize that the high R_{free} value may be due a small but significant amount of degradation that is observed during the purification process.

The lipoate-bound *PfLipL1* _{Δ 243–279} structure [Fig. 1(A)] consists of a large N-terminal domain (NTD, residues 21–276), a linker region lacking defined secondary structure (residues 277–289), and a small C-terminal domain (CTD, residues 290–370). The NTD contains two β -sheets, a large mixed β -sheet made up of seven β -strands (β 1, β 2, β 6, β 7, β 8, β 9, and β 10) and a small

**Figure 1**

Overall structure and binding pocket of lipoyl-bound *PfLipL1* $_{\Delta 243-279}$. (A) Cartoon representation of chain A of lipoyl-bound *PfLipL1* $_{\Delta 243-279}$. Secondary structure elements are labeled and the lipoyl moiety is shown in stick representation. Important residues for the binding pocket are shaded in red and blue for residues contributing hydrophobic and H-bond interactions, respectively. (B) Superposition of chain A (cyan) and chain B (red) of lipoyl-bound *PfLipL1* $_{\Delta 243-279}$. The major differences in the two monomers are the lack of density for the loop defined by residues 242–247 and the extension of the adenylate-binding loop. (C) LIDIA representation of the binding site of Chain A. Residues involved in hydrophobic interactions are represented as lime green circles and residues involved in H-bond interactions are represented as blue or green dashed lines for main chain or side-chain interactions, respectively. (D and E) Surface representation of the lipoyl binding pocket. Important residues are shown in stick representation and colored blue or red for H-bonds or hydrophobic interactions, respectively. H-bonds are represented as blue dashed lines.

mixed-sheet made up of three strands ($\beta 3$, $\beta 4$, and $\beta 5$). There are six α -helical elements surrounding the β -sheets ($\alpha 1$ – $\alpha 6$). The CTD consists of one anti-parallel β -sheet made up of three strands ($\beta 11$, $\beta 12$, and $\beta 13$) and three α -helices ($\alpha 7$, $\alpha 8$, and $\alpha 9$). The two monomers in the asymmetric unit are in similar conformations and superimpose with a root-mean-square deviation

(r.m.s.d.) of 0.4 Å for the corresponding 269 C α atoms [Fig. 1(B)]. The most notable differences between the two monomers are a lack of density in Chain B residues 242–247 (a flexible loop at the site of the deletion) and an extension of the Chain B adenylate-binding loop at residues 194–200. The latter extension forms a β -strand with a symmetry-related monomer.

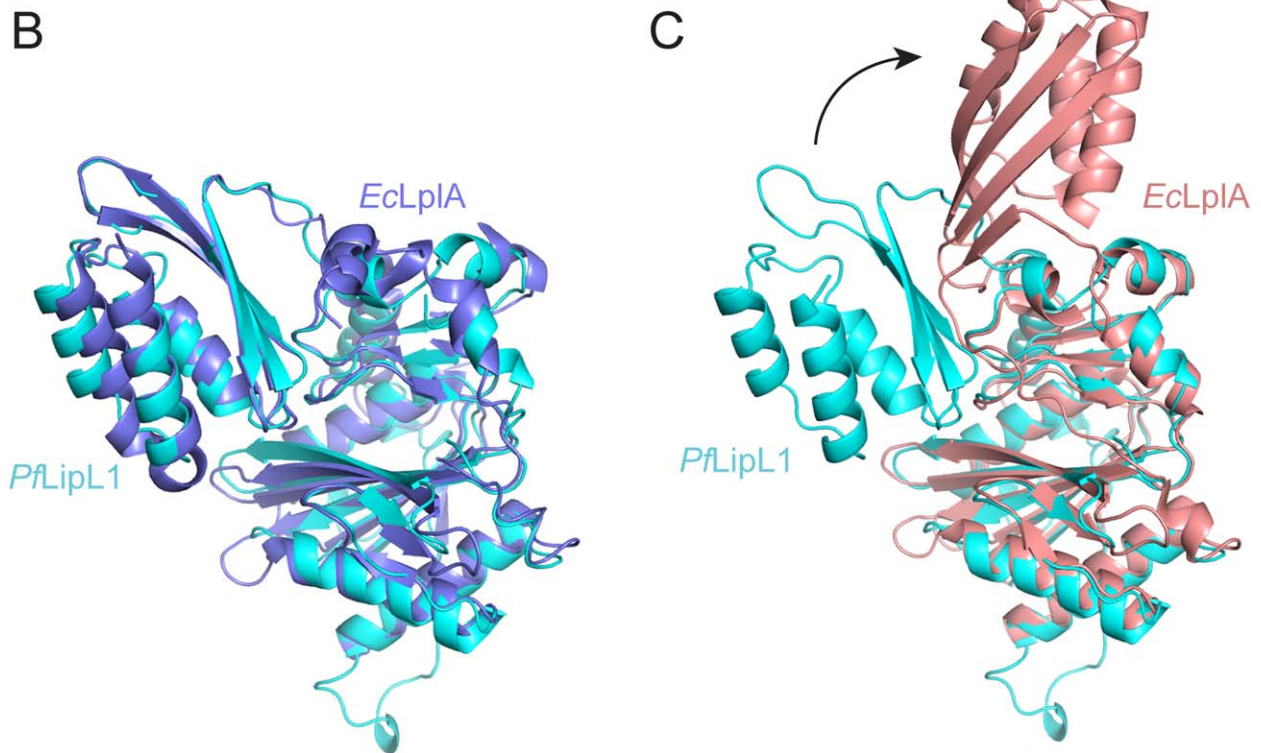
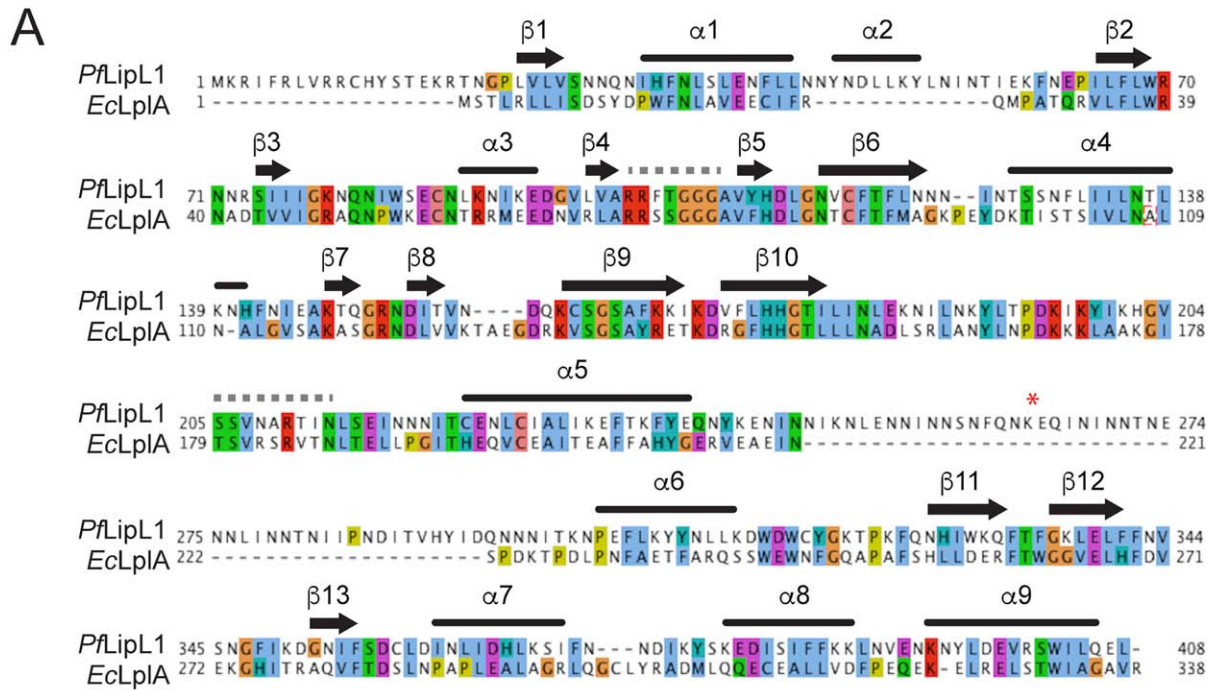


Figure 2

Comparison of *PfLipL1* and *EcLpIA*. (A) Clustal sequence alignment of full-length *PfLipL1* and *EcLpIA*. Residues are colored using the ClustalX color scheme. Secondary structure elements are labeled as follows: arrows represent β -strands and rectangles represent α -helices. The lipote-binding loop is highlighted with a grey-dashed line between $\beta 4$ and $\beta 5$ and the adenylate-binding loop is highlighted with a grey dashed line between $\beta 10$ and $\alpha 5$. The site of proteolytic cleavage in full length *PfLipL1* is marked with a red asterisk. (B) Overlay of lipote-bound *PfLipL1* _{$\Delta 243-279$} , colored cyan, and lipote-bound *EcLpIA* (PDB 1X2H), colored slate generated by the RAPIDO server.^{36,37} Both structures are considered to be in the “bent” conformation which is incompatible with binding substrate proteins. (C) Overlay of lipote-bound *PfLipL1* _{$\Delta 243-279$} , colored cyan, and lipoyl-AMP-bound *EcLpIA* (PDB 3A7R), colored salmon. The CTD of *EcLpIA* has translated approximately 90° and rotated approximately 180° to accommodate substrate enzyme binding. It is of interest to note the formation of a small β -strand in the CTD from residues that belong to the long adenylate-binding loop.

Figure 1(C) shows the LIDIA diagram of the lipoate-binding site in Chain A of the *PfLipL1* $_{\Delta 243-279}$ structure.³² Here, residues that are involved in hydrophobic interactions are shown in lime green and residues involved in H-bond interactions are shown as blue and green dashed lines for main chain and side-chain interactions, respectively. It is important to note one additional difference between Chain A and Chain B in reference to the lipoate-binding site. In Chain B, it is the side-chain of residue N152 as opposed to the amide hydrogen of residue G107 that forms the second hydrogen bond with the lipoate carboxylate.

Figure 1(D,E) shows the close-up view of the lipoate-binding pocket of *PfLipL1* $_{\Delta 243-279}$, where residues that show significant interactions with the lipoate moiety are highlighted in stick representation and colored red (hydrophobic interactions) or blue (H-bond interactions). The pocket is defined by interactions with residues from $\beta 2$, $\beta 5$, $\beta 9$, $\beta 10$, and the loop region between $\beta 4$ and $\beta 5$, known as the lipoate-binding loop (residues 101–106). The lipoate-binding loop is a hallmark of all lipoate protein ligases and lipoate transferases. It is of special interest to highlight the hydrogen bonding interaction between the lipoate carbonyl and residue K160. Lipoate ligase enzymes are characterized by having an active site lysine that forms hydrogen bonds with both lipoate and ATP orienting the carboxylate of lipoate for a nucleophilic attack on the α -phosphorus atom of ATP.³³ Indeed, an alanine substitution of K160 renders full-length *PfLipL1* unable to form lipoyl-AMP and abrogates lipoylation activity *in vitro*.¹⁴

Structure comparison

We searched for proteins with structural similarity to *PfLipL1* $_{\Delta 243-279}$ using the Dali server.²⁶ Generally, the Dali server measures similarity by a sum-of-pairs method that results in a Dali-Z score. Structures with a Dali-Z score above 2 are considered to have significant similarity and will usually be characterized as having similar folds. The top scoring result from the Dali server for *PfLipL1* $_{\Delta 243-279}$ is a computationally designed resorfin ligase that was designed based on the *EcLplA* scaffold (PDB: 4TVY, Z-score: 32.4).³⁴ Additionally, apo-bound, lipoate-bound, and lipoyl-AMP-bound *EcLplA* structures also have a high Z-score in the Dali server results (PDBs: 1X2G, 1X2H, 3A7R; Z-scores: 31.1, 31.1, 30.5, respectively). A sequence alignment of *PfLipL1* $_{\Delta 243-279}$ and *EcLplA* shows all secondary structure elements to be conserved and a percentage identity of 29.8% [Fig. 2(A)].

The structure of lipoate-bound *PfLipL1* $_{\Delta 243-279}$ is in the same “bent” conformation as the *EcLplA* structure in the “unliganded” form [Fig. 2(B)].^{33,35} In this conformation, the CTD is bent such that it obscures the putative H-protein-binding site in a similar mechanism as

that observed for *EcLplA*.³³ This conformation is characterized by a hydrogen bond between the amide of G106 of the lipoate-binding loop and the carbonyl of C321 in the CTD. Additionally, there is a conserved salt-bridge between residues K79 in the NTD and D328 in the CTD. Similar interactions can also be observed in the *EcLplA* structures in the “bent” conformation. Comparison of the lipoate-bound *PfLipL1* $_{\Delta 243-279}$ to lipoyl-AMP-bound *EcLplA* [Fig. 2(C)] shows that a large structural rearrangement must occur in *PfLipL1* $_{\Delta 243-279}$ to accommodate H-protein for lipoylation.

PfLipL1 deletion mutants are characterized by wild-type-like lipoylation activity *in vitro*

Although full-length *PfLipL1* can be easily expressed and purified from *E. coli* with high yield, this construct is prone to spontaneous proteolytic cleavage. Amino acid sequencing revealed that cleavage initially occurs between K264 and E265 (data not shown); however, alanine substitution at position 264 does not prevent degradation even in the presence of protease inhibitors (data not shown). *PfLipL1* contains a low complexity region that is not conserved in other characterized lipoate ligases and despite the presence of this region in other *Plasmodium* species there is no conservation of sequence or size. Full-length *PfLipL1* crystals can still be generated but only diffract to low resolution. We therefore decided to make a series of mutations that removed the low complexity sequence from our construct and tested the mutant *PfLipL1* constructs both in a cell-based lipoylation assay and an *in vitro* lipoylation assay. We made three different deletion mutants removing 5, 10, or 15 residues on both sides of K264 (deleting a total of 11, 21, or 31 amino acids, respectively). These constructs still suffered from degradation, prompting us to make a fourth deletion (*PfLipL1* $_{\Delta 243-279}$) removing more residues from the low complexity loop. The latter construct, *PfLipL1* $_{\Delta 243-279}$, shows minor degradation but is far more stable than the full-length construct. All loop deletion constructs appear to be enzymatically active. Indeed, *E. coli* substrate proteins are lipoylated when all *PfLipL1* variants are expressed in a lipoylation-deficient cell line (Supporting Information, Fig. S1A). Furthermore, *in vitro* lipoylation of the *PfH* protein, a canonical substrate enzyme, remains unchanged in the *PfLipL1* $_{\Delta 243-279}$ deletion mutant (Supporting Information, Fig. S1B). As the lipoylation activity of all *PfLipL1* variants remains unchanged with deletion of the low complexity region, the *PfLipL1* $_{\Delta 243-279}$ construct is likely a good structural surrogate to understand the mechanism of lipoylation in *P. falciparum*.

ACKNOWLEDGMENTS

The contents of this publication are solely the responsibility of the authors and do not necessarily represent

the official views of NIGMS or NIH. The authors declare no conflict of interest.

REFERENCES

- Mudhune SA, Okiro EA, Noor AM, Zurovac D, Juma E, Ochola SA, Snow RW. The clinical burden of malaria in Nairobi: a historical review and contemporary audit. *Malaria J* 2011;10:138.
- Okiro EA, Al-Taiar A, Reyburn H, Idro R, Berkley JA, Snow RW. Age patterns of severe paediatric malaria and their relationship to *Plasmodium falciparum* transmission intensity. *Malaria J* 2009;8:4.
- Okiro EA, Bitira D, Mbazizi G, Mpimbaza A, Alegana VA, Talisuna AO, Snow RW. Increasing malaria hospital admissions in Uganda between 1999 and 2009. *BMC Med* 2011;9:37.
- Delves M, Plouffe D, Scheurer C, Meister S, Wittlin S, Winzeler EA, Sinden RE, Leroy D. The activities of current antimalarial drugs on the life cycle stages of *Plasmodium*: a comparative study with human and rodent parasites. Beeson JG, editor. *PLoS Med* 2012;9:e1001169.
- Fidock DA, Eastman RT, Ward SA, Meshnick SR. Recent highlights in antimalarial drug resistance and chemotherapy research. *Trends Parasitol* 2008;24:537–544.
- Dondorp AM, Fairhurst RM, Slutsker L, Macarthur JR, Breman JG, Guerin PJ, Wellems TE, Ringwald P, Newman RD, Plowe CV. The threat of artemisinin-resistant malaria. *N Engl J Med* 2011;365:1073–1075.
- Phyo AP, Nkhoma S, Stepniewska K, Ashley EA, Nair S, McGready R, ler Moo C, Al-Saai S, Dondorp AM, Lwin KM, et al. Emergence of artemisinin-resistant malaria on the western border of Thailand: a longitudinal study. *Lancet (London, England)* 2012;379:1960–1966.
- Allary M, Lu JZ, Zhu L, Prigge ST. Scavenging of the cofactor lipoate is essential for the survival of the malaria parasite *Plasmodium falciparum*. *Mol Microbiol* 2007;63:1331–1344.
- Spalding MD, Prigge ST. Lipoic acid metabolism in microbial pathogens. *Microbiol Mol Biol Rev* 2010;74:200–228.
- Wrenger C, Müller S. The human malaria parasite *Plasmodium falciparum* has distinct organelle-specific lipoylation pathways. *Mol Microbiol* 2004;53:103–113.
- Foth BJ, Ralph SA, Tonkin CJ, Struck NS, Fraunholz M, Roos DS, Cowman AF, McFadden GI. Dissecting apicoplast targeting in the malaria parasite *Plasmodium falciparum*. *Science* 2003;299:705–708.
- Falkard B, Kumar TRS, Hecht L-S, Matthews KA, Henrich PP, Gulati S, Lewis RE, Manary MJ, Winzeler EA, Sinnis P, et al. A key role for lipoic acid synthesis during *Plasmodium* liver stage development. *Cell Microbiol* 2013;15:1585–1604.
- Deschermeier C, Hecht L-S, Bach F, Rützel K, Stanway RR, Nagel A, Seeber F, Heussler VT. Mitochondrial lipoic acid scavenging is essential for *Plasmodium berghei* liver stage development. *Cell Microbiol* 2012;14:416–430.
- Afanador GA, Matthews KA, Bartee D, Gisselberg JE, Walters MS, Freel Meyers CL, Prigge ST. Redox-dependent lipoylation of mitochondrial proteins in *Plasmodium falciparum*. *Mol Microbiol* 2014.
- Spalding MD, Allary M, Gallagher JR, Prigge ST. Validation of a modified method for Bxb1 mycobacteriophage integrase-mediated recombination in *Plasmodium falciparum* by localization of the H-protein of the glycine cleavage complex to the mitochondrion. *Mol Biochem Parasitol* 2010;172:156–160.
- Afanador GA, Guerra AJ, Swift RP, Rodriguez RE, Bartee D, Matthews KA, Schön A, Freire E, Freel Meyers CL, Prigge ST. A novel lipoate attachment enzyme is shared by *Plasmodium* and *Chlamydia* species. Submitted.
- Muench SP, Rafferty JB, McLeod R, Rice DW, Prigge ST. Expression, purification and crystallization of the *Plasmodium falciparum* enoyl reductase. *Acta Crystallogr D Biol Crystallogr* 2003;59:1246–1248.
- Kabsch W. Automatic processing of rotation diffraction data from crystals of initially unknown symmetry and cell constants. *J Appl Crystallogr* 1993;26:795–800.
- Kabsch W. Integration, scaling, space-group assignment and post-refinement. *Acta Crystallogr D Biol Crystallogr* 2010;66:133–144.
- Kabsch W. XDS. *Acta Crystallogr D Biol Crystallogr* 2010;66:125–132.
- Adams PD, Afonine PV, Bunkóczi G, Chen VB, Davis IW, Echols N, Headd JJ, Hung LW, Kapral GJ, Grosse-Kunstleve RW, et al. PHENIX: a comprehensive Python-based system for macromolecular structure solution. *Acta Crystallogr D Biol Crystallogr* 2010;66:213–221.
- McCoy AJ, Grosse-Kunstleve RW, Adams PD, Winn MD, Storoni LC, Read RJ. Phaser crystallographic software. *J Appl Crystallogr* 2007;40:658–674.
- Emsley P, Cowtan K. Coot: model-building tools for molecular graphics. *Acta Crystallogr D Biol Crystallogr* 2004;60:2126–2132.
- Chen VB, Arendall WB, Headd JJ, Keedy DA, Immormino RM, Kapral GJ, Murray LW, Richardson JS, Richardson DC. MolProbity: all-atom s validation for macromolecular crystallography. *Acta Crystallogr D Biol Crystallogr* 2010;66:12–21.
- Davis IW, Leaver-Fay A, Chen VB, Block JN, Kapral GJ, Wang X, Murray LW, Arendall WB, Snoeyink J, Richardson JS, et al. MolProbity: all-atom contacts and structure validation for proteins and nucleic acids. *Nucleic Acids Res* 2007;35:W375–W383.
- Holm L, Rosenström P. Dali server: conservation mapping in 3D. *Nucleic Acids Res* 2010;38:W545–W549.
- Clamp M, Cuff J, Searle SM, Barton GJ. The Jalview Java alignment editor. *Bioinformatics* 2004;20:426–427.
- Waterhouse AM, Procter JB, Martin DMA, Clamp M, Barton GJ. Jalview Version 2—a multiple sequence alignment editor and analysis workbench. *Bioinformatics* 2009;25:1189–1191.
- Troshin PV, Procter JB, Barton GJ. Java bioinformatics analysis web services for multiple sequence alignment—JABAWS: MSA. *Bioinformatics* 2011;27:2001–2002.
- Schrödinger LLC. The PyMOL Molecular Graphics System Version 1.8.
- Lebedev AA, Isupov MN. Space-group and origin ambiguity in macromolecular structures with pseudo-symmetry and its treatment with the program Zanuda. *Acta Crystallogr D Biol Crystallogr* 2014;70:2430–2443.
- Emsley P. Tools for ligand validation in Coot. *Acta Crystallogr D Struct Biol* 2017;73:203–210.
- Fujiwara K, Maita N, Hosaka H, Okamura-Ikeda K, Nakagawa A, Taniguchi H. Global conformational change associated with the two-step reaction catalyzed by *Escherichia coli* lipoate-protein ligase A. *J Biol Chem* 2010;285:9971–9980.
- Liu DS, Nivón LG, Richter F, Goldman PJ, Deerinck TJ, Yao JZ, Richardson D, Phipps WS, Ye AZ, Ellisman MH, et al. Computational design of a red fluorophore ligase for site-specific protein labeling in living cells. *Proc Natl Acad Sci USA* 2014;111:E4551–E4559.
- Fujiwara K, Toma S, Okamura-Ikeda K, Motokawa Y, Nakagawa A, Taniguchi H. Crystal structure of lipoate-protein ligase A from *Escherichia coli*. Determination of the lipoic acid-binding site. *J Biol Chem* 2005;280:33645–33651.
- Mosca R, Brannetti B, Schneider TR. Alignment of protein structures in the presence of domain motions. *BMC Bioinformatics* 2008;9:352.
- Mosca R, Schneider TR. RAPIDO: a web server for the alignment of protein structures in the presence of conformational changes. *Nucleic Acids Res* 2008;36:W42–W46.